ACS OMEGA

http://pubs.acs.org/journal/acsodf

Article

Highlighting the Anti-Synergy between Adsorption and Diffusion in Cation-Exchanged Faujasite Zeolites

Rajamani Krishna* and Jasper M. van Baten

Cite This: *ACS Omega* 2022, 7, 13050−13056

Read Online

ACCESS | Metrics & More | Article Recommendations | Supporting Information

ABSTRACT: Using configurational-bias Monte Carlo simulations of adsorption equilibrium and molecular dynamics simulations of guest diffusivities of CO_2, CH_4, N_2, and O_2 in FAU zeolites with varying amounts of extra-framework cations (Na^+ or Li^+), we demonstrate that adsorption and diffusion do not, in general, proceed hand-in-hand. Stronger adsorption often implies reduced mobility. The anti-synergy between adsorption and diffusion has consequences for the design and development of pressure-swing adsorption and membrane separation technologies for CO_2 capture and N_2/O_2 separations.

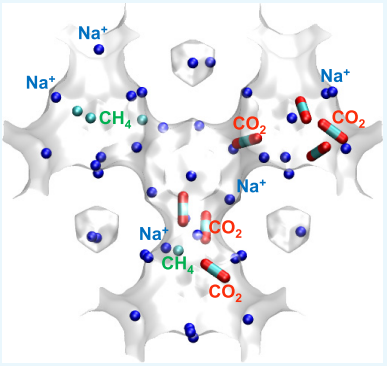

1. INTRODUCTION

Despite the burgeoning research and development activities on novel metal−organic frameworks (MOFs) in separation applications, cation-exchanged zeolites remain viable contenders for use as adsorbents in the industrial practice. For post-combustion CO_2 capture, Na^+ cation-exchanged FAU (faujasite) zeolite, NaX, also commonly known by its trade name 13X (with Si/Al ≈ 1.2), is considered to be the benchmark adsorbent, with the ability to meet government targets for CO_2 purity and recovery.[1] NaX zeolites are also of potential use in natural gas purification,[2,3] alkane/alkene separations,[4−8] and hydrogen purification processes.[3,9−23] Coulombic interactions of CO_2 and unsaturated alkenes with the extra-framework cations (e.g., Na^+, Ca^{++}, Li^+, and Ba^{++}) result in strong binding; the binding strength and selectivity can be tuned by the appropriate choice of the extra-framework cations and the adjustment of the Si/Al ratios.[9,11,20,24−26]

Li^+ cation-exchanged FAU (faujasite) zeolite is commercially used for separation of N_2/O_2 mixtures.[23,27,28] For supplying medical grade oxygen to prevent hypoxemia-related complications related to COVID-19, portable medical oxygen concentrators commonly use LiLSX (LS = low silica; Si/Al ≈ 1) to achieve high N_2/O_2 adsorption selectivities, ensuring enhanced rejection of purified O_2, the desired product.[29,30]

For separation applications using pressure-swing adsorption (PSA) technology, consisting of adsorption/desorption cycles, there is often a mismatch between the requirements of strong adsorption and ease of desorption.[31] For example, NaX has a very strong affinity for CO_2, but the regeneration requires application of deep vacuum. For CO_2 capture from flue gases, Prats et al.[25,26] have used molecular simulations of mixture adsorption in FAU to determine the optimum Si/Al ratio for PSA operations.

In the design and development of PSA technologies employing cation-exchanged zeolite adsorbents, we also require data on the intracrystalline diffusivities of guest molecules. Most commonly, diffusion limitations cause distended breakthrough characteristics and reduction in the purities of the desired products.[31−36] Diffusivity data are also of vital importance in the development of zeolite membrane constructs for mixture separations in which cation-exchanged zeolites are used as thin layers or as fillers in mixed-matrix configurations.[37−43]

The primary objective of this communication is to gain some fundamental thermodynamic insights into the adsorption and diffusion characteristics of a variety of guest molecules such as CO_2, CH_4, N_2, and O_2 in FAU zeolites with varying amounts of extra-framework cations: Na^+ and Li^+. The desired insights are obtained by performing configurational-bias Monte Carlo (CBMC) simulations of adsorption and molecular dynamics (MD) simulations of diffusion in Na- and Li-exchanged FAU zeolites with varying Si/Al ratios. The CBMC and MD simulation methodologies, along with details of the force field implementations, are detailed in the Supporting Information accompanying this publication. We aim to demonstrate the

Received: January 21, 2022
Accepted: March 14, 2022
Published: April 8, 2022

anti-synergy between adsorption and diffusion; the stronger the binding of a guest molecule, the lower is its mobility. Such insights are of vital importance in determining the optimum Si/Al ratio of zeolite for use in PSA technologies or in membrane constructs.

2. THE GIBBSIAN CONCEPT OF SPREADING PRESSURE

The spreading pressure, π, is related to the molar chemical potential, μ_i, by the Gibbs adsorption equation[44]

$$A\mathrm{d}\pi = \sum_{i=1}^{n} q_i \mathrm{d}\mu_i \tag{1}$$

where A represents the surface area per kg of framework, and q_i is the component molar loading in the adsorbed phase mixture. At thermodynamic equilibrium, the μ_i are related to the partial fugacities in the bulk fluid mixture

$$\mathrm{d}\mu_i = RT\mathrm{d}\ln f_i \tag{2}$$

In developing the ideal adsorbed solution theory (IAST), Myers and Prausnitz[45] write the following expression relating the partial fugacities in the bulk gas mixture

$$f_i = P_i^0 x_i; \quad i = 1, 2, ..., n \tag{3}$$

to the mole fractions, x_i, in the adsorbed phase mixture

$$x_i = \frac{q_i}{q_1 + q_2 + ... + q_n}; \quad i = 1, 2, ..., n \tag{4}$$

In eq 3, P_i^0 is the pressure for sorption of every component i, which yields the same spreading pressure, π, for each of the pure components as that for the n-component mixture:

$$\frac{\pi A}{RT} = \int_0^{P_1^0} \frac{q_1^0(f)}{f}\mathrm{d}f = \int_0^{P_2^0} \frac{q_2^0(f)}{f}\mathrm{d}f = \int_0^{P_3^0} \frac{q_3^0(f)}{f}\mathrm{d}f \tag{5}$$

In eq 5, $q_i^0(f)$ is the pure component adsorption isotherm. Since the surface area A is not directly accessible from experimental data, the surface potential $\pi A/RT \equiv \Phi$, with the units mol kg^{-1}, serves as a convenient and practical proxy for the spreading pressure π.[46−49] As derived in detail in the Supporting Information, the fractional pore occupancy, θ, is related to the surface potential by

$$\theta = 1 - \exp\left(-\frac{\Phi}{q_{\mathrm{sat,mix}}}\right) \tag{6}$$

where $q_{\mathrm{sat,\,mix}}$ is the saturation capacity for mixture adsorption. Equation 6 implies that Φ may also be interpreted as a proxy for the pore occupancy; it is the fundamentally correct yardstick to compare the adsorption and diffusion characteristics of different host materials.[41,48−50]

In view of eq 3, we may express the adsorption selectivity for the i−j pair as follows

$$S_{\mathrm{ads}} = \frac{q_i/q_j}{f_i/f_j} = \frac{x_i/f_i}{x_j/f_j} = \frac{P_j^0}{P_i^0} \tag{7}$$

Applying the restriction specified by eq 5, it follows that S_{ads} is uniquely determined by the surface potential Φ, irrespective of the mixture composition and total fugacity, f_t.

3. RESULTS AND DISCUSSION

3.1. CO_2 Capture Using Na-Exchanged FAU. Figure 1a plots the CBMC data on isosteric heats of adsorption, Q_{st}, a measure of the binding energies, of CO_2 and CH_4 in FAU (0 Al, all-silica), NaY (54 Al uc^{-1}), and NaX (86 Al uc^{-1}) zeolites, plotted as a function of the surface potential Φ. For CO_2, the hierarchy of Q_{st} is NaX > NaY > FAU; this hierarchy reflects the strong electrostatic interactions with the extra-framework cations, engendered by the large quadrupole moment of CO_2. For CH_4, the differences in the Q_{st} in the three different hosts are considerably smaller because the adsorption of CH_4 is due to van der Waals interactions that also increase with increasing number of cations.

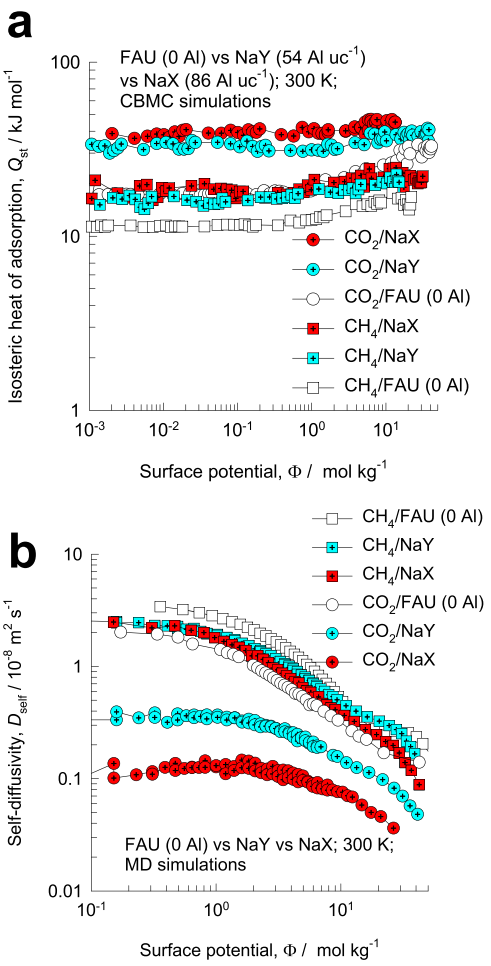

Figure 1. (a) CBMC simulations of the isosteric heats of adsorption, Q_{st}, of CO_2 and CH_4 in FAU (0 Al, all-silica), NaY (54 Al uc^{-1}), and NaX (86 Al uc^{-1}) zeolites, determined at 300 K, plotted as a function of the surface potential Φ. (b) MD simulations of the self-diffusivities, $D_{i,\,\mathrm{self}}$, of CO_2 and CH_4 in FAU, NaY, and NaX zeolites, determined at 300 K, plotted as a function of the surface potential Φ. All simulation details and input data are provided in the Supporting Information accompanying this publication.

Strong binding of guest molecules also implies a higher degree of "stickiness" and, consequently, lower mobility.[51,52] To demonstrate this, Figure 1b presents the MD simulations of

https://doi.org/10.1021/acsomega.2c00427
ACS Omega 2022, 7, 13050−13056

the unary self-diffusivities, $D_{i,\,self}$, of CO_2 and CH_4 in FAU (0 Al), NaY, and NaX zeolites. Compared at the same surface potential Φ, the hierarchy of self-diffusivities is precisely reverse of the hierarchy of Q_{st}. Noteworthily, CH_4, the guest with the larger kinetic diameter of 3.8 Å, has a higher mobility than CO_2, which has a smaller kinetic diameter of 3.3 Å. The fallacy of using kinetic diameters to anticipate hierarchies in the diffusivity values has been underscored in published works.[15,51]

CBMC simulations were carried out for equimolar ($f_1 = f_2$) $CO_2(1)/CH_4(2)$ mixtures in FAU (0 Al), NaY, and NaX zeolites. The values of the adsorption selectivities, S_{ads}, are plotted in Figure 2a as a function of Φ. The hierarchy of S_{ads} values is NaX > NaY > FAU (0 Al), reflecting the stronger binding of CO_2. The corresponding hierarchy of diffusion selectivities, $S_{diff} = D_{1,\,self}/D_{2,\,self}$, is precisely the reverse of S_{ads}; evidently, mixture adsorption and diffusion do not proceed hand-in-hand. This anti-synergy has important consequences of use of cation-exchanged zeolites in membrane constructs. If the partial fugacities of the components at the downstream face are negligibly small in comparison with those at the upstream face, the component permeabilities may be estimated from the following expression[41]

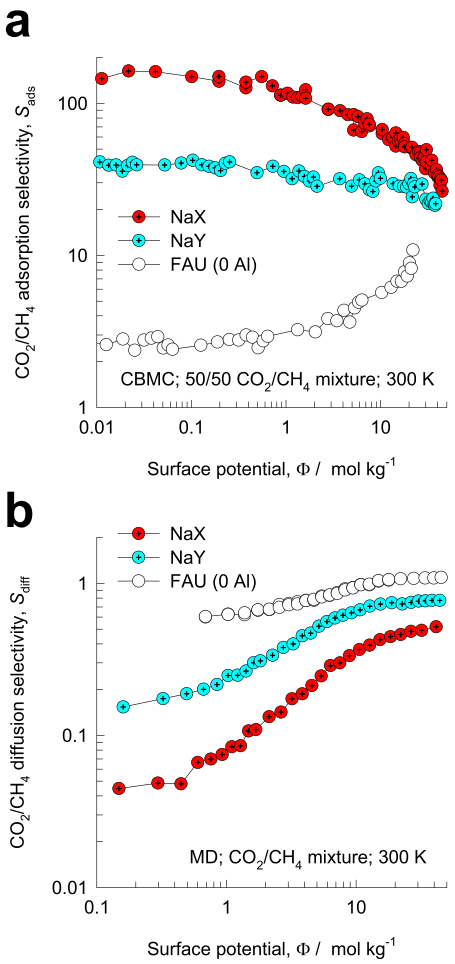

Figure 2. Comparison of CBMC/MD simulations of (a) adsorption selectivities, S_{ads}, and (b) diffusion selectivities, S_{diff}, of CO_2/CH_4 mixtures in FAU (0 Al), NaY, and NaX zeolites at 300 K. The selectivities are plotted as a function of the surface potential Φ. All simulation details and input data are provided in the Supporting Information accompanying this publication.

$$\Pi_i = \frac{\rho D_{i,\mathrm{self}} q_i}{f_i} \tag{8}$$

For FAU (0 Al), NaY, and NaX zeolites, Figure 3a,b compares the values of the CO_2 permeabilities, Π_1, and the permeation selectivity

$$S_{perm} = \Pi_1/\Pi_2 = S_{ads} \times S_{perm} \tag{9}$$

The CO_2 permeabilities, Π_1, decrease with increasing values of Φ. The S_{perm} is a product of the adsorption selectivity and diffusion selectivity (cf. Figure 2a,b). While the S_{diff} increases with Φ for all three hosts, the S_{ads} increases with Φ until a maximum is reached for NaX and NaY and decreases on a further increase in Φ. Consequently, the S_{perm} also shows a maximum value for NaX and NaY. For the specific choice of upstream operating conditions, $f_t = f_1 + f_2 = 10^6$ Pa, Figure 3c shows the Robeson[53] plot of S_{perm} vs Π_1 for the three host structures. We note that the performances of both NaY and NaX lie above the line representing the Robeson upper bound.[53] Since both S_{perm} and Π_1 are important metrics governing the choice of the appropriate membrane material, there is room for optimization of the Si/Al ratio depending on the relative weightage to be assigned to permeation selectivity and permeability. CBMC/MD data that are analogous to those presented in Figures 2 and 3 are obtained for CO_2/N_2, CO_2/H_2, CH_4/H_2, CH_4/C_2H_6, and CH_4/C_3H_8 mixtures in FAU (0 Al), NaY, and NaX (see Figures S60−S64 of the Supporting Information).

3.2. N_2/O_2 Separations Using Li-FAU and Na-FAU.

Figure 4a presents MD simulations of the unary self-diffusivities, $D_{i,\,self}$, for N_2, at 300 K in Li-exchanged FAU zeolites, with different Al contents per unit cell: 0, 48, 54, 86, and 96, plotted as functions of the surface potential Φ; the contents of Li^+ are equal to that of Al. The magnitudes of $D_{i,\,self}$ decrease with increasing values of Φ, which also serves as a proxy for the pore occupancy. At any specified value of Φ, the values of the self-diffusivity, $D_{i,\,self}$, show the following trend: FAU (0 Al) ≫ FAU (48 Al) ≈ FAU (54 Al) > FAU (86 Al) ≈ FAU (96 Al). This hierarchy of $D_{i,\,self}$ values correlates, inversely, with the corresponding values of the isosteric heats of adsorption of N_2 (cf. Figure 4b). N_2 has a significant quadrupole moment, and the electrostatic interaction potentials increase with increasing Al content, leading to increasing binding energies. The data in Figure 4a,b confirm that the diffusional mobility of N_2 is reduced with increased binding energy.

On the other hand, we note from Figure 4b that the isosteric heats of adsorption of O_2 are practically uninfluenced by the addition of extra-framework cations due to the significantly lower quadrupole moment of O_2. Therefore, we should anticipate that the mobility of O_2 should be practically independent of the degree of Li exchange; this expectation is fulfilled by the MD simulations of the self-diffusivities of O_2 in Li-FAU (see Figure 4c).

For 80/20 N_2/O_2 mixture adsorption, Figure 5a plots the adsorption selectivities, S_{ads}, of Li-exchanged FAU zeolites, with different Al contents. We note that the S_{ads} increases with increasing Al content. MD simulations of the N_2/O_2 diffusion selectivities, S_{diff}, plotted in Figure 5b, demonstrate the anti-synergy between adsorption and diffusion; the higher the

https://doi.org/10.1021/acsomega.2c00427
ACS Omega 2022, 7, 13050−13056

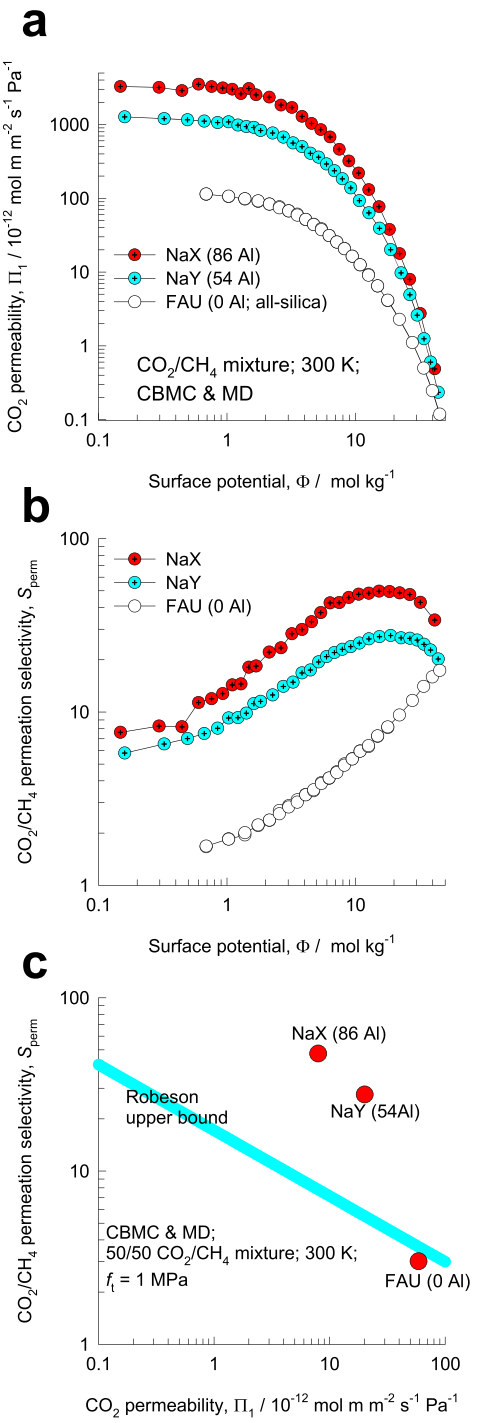

Figure 3. Comparison of (a) CO_2 permeability, Π_1, and (b) permeation selectivity, S_{perm}, for $CO_2(1)/CH_4(2)$ mixtures in FAU (0 Al), NaY, and NaX zeolites at 300 K; the x-axis represents the surface potential Φ. (c) Robeson plot of S_{perm} vs Π_1 data at $f_t = f_1 + f_2 = 10^6$ Pa and 300 K. All simulation details and input data are provided in the Supporting Information accompanying this publication.

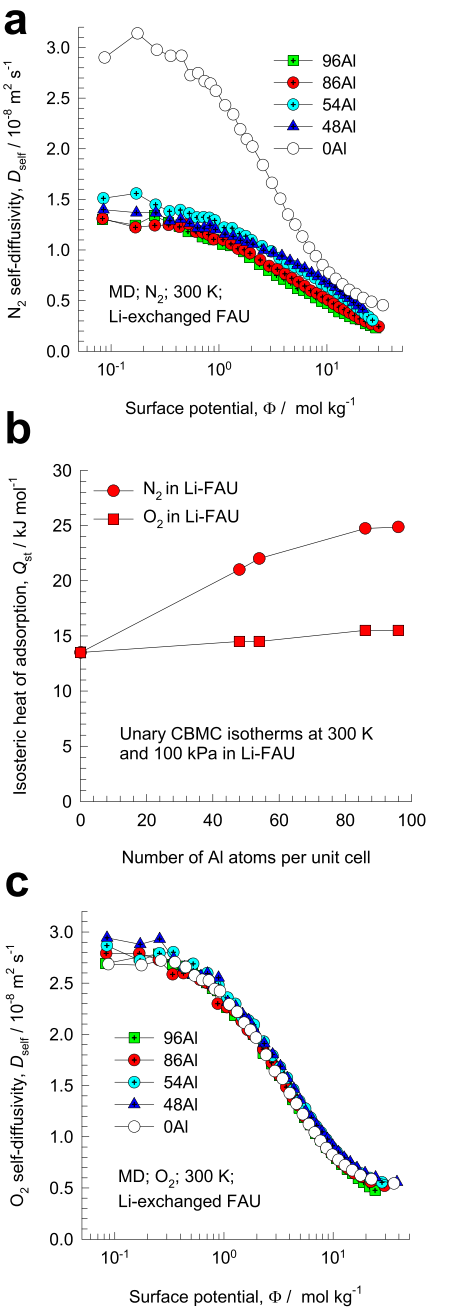

Figure 4. (a) MD simulations of the unary self-diffusivities for N_2 at 300 K in Li-exchanged FAU zeolites, with different Al contents per unit cell: 0, 48, 54, 86, and 96, plotted as a function of the surface potential Φ. (b) Isosteric heats of adsorption, Q_{st}, plotted as a function of the number of Al atoms per unit cell. (c) MD simulations of the unary self-diffusivities for O_2 at 300 K in Li-exchanged FAU zeolites, with different Al contents per unit cell: 0, 48, 54, 86, and 96, plotted as a function of the surface potential Φ. All simulation details and input data are provided in the Supporting Information accompanying this publication.

adsorption selectivity, the lower is the corresponding diffusion selectivity. Analogous CBMC and MD simulations with Na-exchanged FAU zeolites were also carried out; the results are provided in Figures S73−S81 of the Supporting Information.

For 80/20 N_2/O_2 mixture separations at a total fugacity of 100 kPa, Figure 6a compares the adsorption selectivities of Li-FAU and Na-FAU. For the same Al content, we note that the S_{ads} values with Li-FAU are significantly higher than for Na-FAU. The interaction potential, engendered by the quadrupole moment, is inversely proportional to the cube of the center-to-center distance between nitrogen molecules and the extra-framework cation (see the detailed explanation provided in Chapter 2 of the Supporting Information). Due to the smaller ionic radius of Li^+, compared to Na^+, the N_2-Li^+ distances are smaller than the N_2-Na^+ distances; this is confirmed by radial

https://doi.org/10.1021/acsomega.2c00427
ACS Omega 2022, 7, 13050−13056

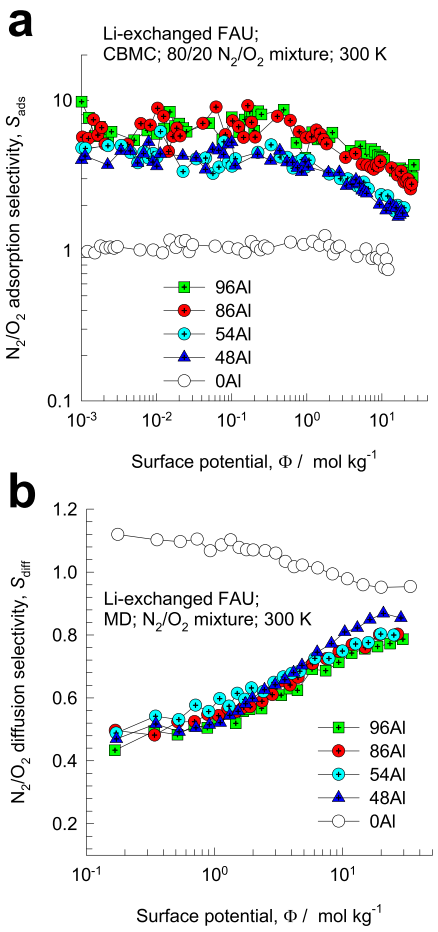

Figure 5. (a) CBMC simulations of the adsorption selectivity, S_{ads}, for binary 80/20 N_2/O_2 mixture adsorption in Li-FAU, with different Al contents per unit cell: 0, 48, 54, 86, and 96. (b) MD simulations of the N_2/O_2 diffusion selectivity, S_{diff}, at 300 K in Li-FAU zeolites. All simulation details and input data are provided in the Supporting Information accompanying this publication.

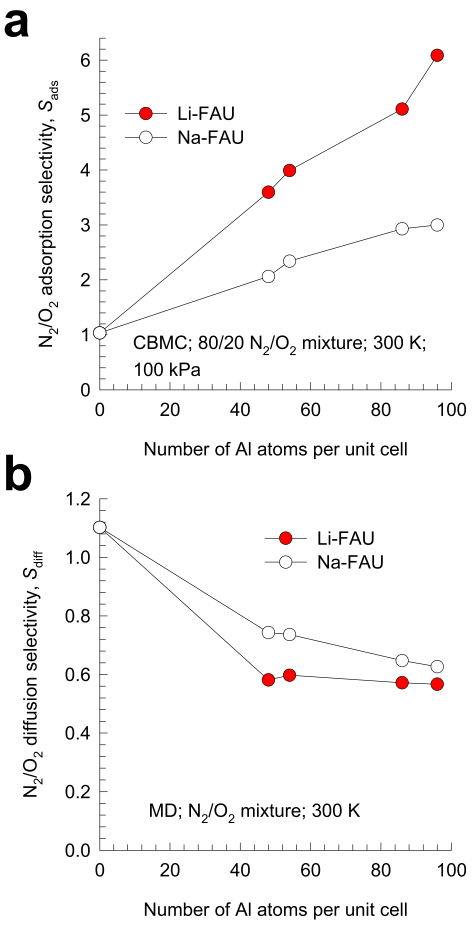

Figure 6. Comparison of the (a) adsorption selectivity and (b) diffusion selectivity for 80/20 N_2/O_2 separations using either Li-exchanged or Na-exchanged FAU zeolites, with different Al contents per unit cell: 0, 48, 54, 86, and 96. All simulation details and input data are provided in the Supporting Information accompanying this publication.

distribution functions for N_2−Li^+ and N_2−Na^+ pairs for 80/20 N_2/O_2 mixture adsorption in Li-FAU(96Al) and Na-FAU-(96Al) (see Figure 7).

The N_2/O_2 diffusion selectivities for Na-FAU are only slightly higher than those of Li-FAU (see Figure 6b). The CBMC/MD data rationalize the use of LiX, with Al ≈ 96 uc^{-1}, in the industrial practice.[29,30]

Figure 8 shows a Robeson plot of S_{perm} vs N_2 permeabilities of N_2 for binary 80/20 N_2/O_2 mixture permeation across the Li-FAU zeolite membrane at an upstream total pressure of 100 kPa. We note that the separation performance increases monotonously with increasing degrees of Li^+ exchange; the permeabilities are significantly higher than the values reported in the literature[54] for polymeric and mixed-matrix membranes.

4. CONCLUSIONS

A combination of CBMC and MD simulations for adsorption and diffusion of guest molecules CO_2, CH_4, N_2, and O_2 in FAU zeolites with varying amounts of extra-framework cations (Na^+ or Li^+) was carried out to investigate the influence of varying Si/Al ratios on mixture separations. Stronger adsorption, with increasing amounts of extra-framework cations, results in lowered diffusivities. For CO_2/CH_4 and N_2/O_2 mixture separations, the adsorption selectivity, S_{ads}, and diffusion selectivity, S_{diff}, do not proceed hand-in-hand. The anti-synergy between adsorption and diffusion has important consequences for the choice of the extra-framework cation, Na^+ or Li^+, and the Si/Al ratio for use in PSA and membrane separation technologies.

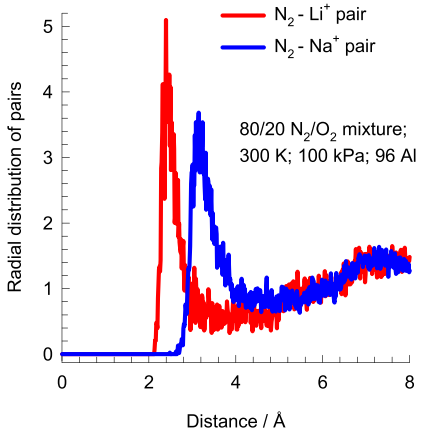

Figure 7. Radial distribution functions for N_2−Li^+ and N_2−Na^+ pairs for 80/20 N_2/O_2 mixture adsorption in Li-FAU (96Al) and Na-FAU (96Al) at 100 kPa and 300 K.

https://doi.org/10.1021/acsomega.2c00427
ACS Omega 2022, 7, 13050−13056

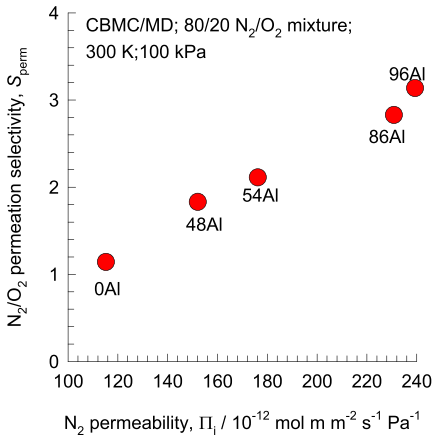

Figure 8. Robeson plot of S_{perm} vs N_2 permeabilities for binary 80/20 N_2/O_2 mixture permeation across the Li-exchanged FAU zeolite membrane, with different Al contents per unit cell: 0, 48, 54, 86, and 96. All simulation details and input data are provided in the Supporting Information accompanying this publication.

■ ASSOCIATED CONTENT

Supporting Information

The Supporting Information is available free of charge at https://pubs.acs.org/doi/10.1021/acsomega.2c00427.

CBMC and MD simulation methodologies; details of IAST calculations; Maxwell−Stefan formulation for mixture diffusion; CBMC data on unary isotherms and isotherm fits; CBMC and MD data on adsorption, diffusion, and permeation of mixtures in various cation-exchanged FAU zeolites (PDF)

■ AUTHOR INFORMATION

Corresponding Author

Rajamani Krishna − *Van't Hoff Institute for Molecular Sciences, University of Amsterdam, 1098 XH Amsterdam, The Netherlands;* orcid.org/0000-0002-4784-8530; Email: r.krishna@contact.uva.nl

Author

Jasper M. van Baten − *Van't Hoff Institute for Molecular Sciences, University of Amsterdam, 1098 XH Amsterdam, The Netherlands*

Complete contact information is available at: https://pubs.acs.org/10.1021/acsomega.2c00427

Notes

The authors declare no competing financial interest.

■ ACKNOWLEDGMENTS

The authors acknowledge Dr. Richard Baur for helpful discussions.

■ NOMENCLATURE

Latin Alphabet

A surface area per kg of framework, $m^2\ kg^{-1}$
$D_{i,self}$ self-diffusivity of species i, $m^2\ s^{-1}$
f_i partial fugacity of species i, Pa
f_t total fugacity of bulk gas mixture, Pa
P_i^0 sorption pressure, Pa
q_i component molar loading of species i, $mol\ kg^{-1}$
$q_{i,sat}$ molar loading of species i at saturation, $mol\ kg^{-1}$
Q_{st} isosteric heat of adsorption, $J\ mol^{-1}$
R gas constant, 8.314 $J\ mol^{-1}\ K^{-1}$
S_{ads} adsorption selectivity, dimensionless
S_{diff} diffusion selectivity, dimensionless
S_{perm} permeation selectivity, dimensionless
T absolute temperature, K
x_i mole fraction of species i in the adsorbed phase, dimensionless

Greek Alphabet

μ_i molar chemical potential of component i, $J\ mol^{-1}$
π spreading pressure, $N\ m^{-1}$
θ fractional occupancy, dimensionless
Π_i membrane permeability of species i, $mol\ m\ m^{-2}\ s^{-1}\ Pa^{-1}$
ρ crystal framework density, $kg\ m^{-3}$
Φ surface potential, $mol\ kg^{-1}$

■ REFERENCES

(1) Wilkins, N. S.; Rajendran, A. Measurement of competitive CO_2 and N_2 adsorption on Zeolite 13X for post-combustion CO_2 capture. *Adsorption* **2019**, *25*, 115−133.

(2) Wu, H.; Yao, K.; Zhu, Y.; Li, B.; Shi, Z.; Krishna, R.; Li, J. Cu-TDPAT, an *rht*-type Dual-Functional Metal−Organic Framework Offering Significant Potential for Use in H_2 and Natural Gas Purification Processes Operating at High Pressures. *J. Phys. Chem. C* **2012**, *116*, 16609−16618.

(3) Belmabkhout, Y.; Pirngruber, G.; Jolimaitre, E.; Methivier, A. A complete experimental approach for synthesis gas separation studies using static gravimetric and column breakthrough experiments. *Adsorption* **2007**, *13*, 341−349.

(4) He, Y.; Krishna, R.; Chen, B. Metal-Organic Frameworks with Potential for Energy-Efficient Adsorptive Separation of Light Hydrocarbons. *Energy Environ. Sci.* **2012**, *5*, 9107−9120.

(5) Da Silva, F. A.; Rodrigues, A. E. Vacuum swing adsorption for propylene/propane separation with 4A zeolite. *Ind. Eng. Chem. Res.* **2001**, *40*, 5758−5774.

(6) Grande, C. A.; Poplow, F.; Rodrigues, A. E. Vacuum pressure swing adsorption to produce polymer-grade polypropylene. *Sep. Sci. Technol.* **2010**, *45*, 1252−1259.

(7) Divekar, S.; Nanoti, A.; Dasgupta, S.; Aarti; Chauhan, R.; Gupta, P.; Garg, M. O.; Singh, S. P.; Mishra, I. M. Adsorption Equilibria of Propylene and Propane on Zeolites and Prediction of Their Binary Adsorption with the Ideal Adsorbed Solution Theory. *J. Chem. Eng. Data* **2016**, *61*, 2629−2637.

(8) Da Silva, F. A.; Rodrigues, A. E. PropylenePropane Separation by Vacuum Swing Adsorption Using 13X Zeolite. *AIChE J.* **2001**, *47*, 341−357.

(9) Pirngruber, G. D.; Carlier, V.; Leinekugel-le-Cocq, D. Post-Combustion CO_2 Capture by Vacuum Swing Adsorption Using Zeolites − a Feasibility Study. *Oil Gas Sci. Technol.* **2014**, *69*, 989−1003.

(10) Yang, J.; Krishna, R.; Li, J.; Li, J. Experiments and Simulations on Separating a CO_2/CH_4 Mixture using K-KFI at Low and High Pressures. *Microporous Mesoporous Mater.* **2014**, *184*, 21−27.

(11) Palomino, M.; Corma, A.; Rey, F.; Valencia, S. New Insights on CO_2−Methane Separation Using LTA Zeolites with Different Si/Al Ratios and a First Comparison with MOFs. *Langmuir* **2010**, *26*, 1910−1917.

(12) Krishna, R.; van Baten, J. M. In Silico Screening of Zeolite Membranes for CO_2 Capture. *J. Membr. Sci.* **2010**, *360*, 323−333.

(13) Krishna, R.; van Baten, J. M. In silico screening of metal-organic frameworks in separation applications. *Phys. Chem. Chem. Phys.* **2011**, *13*, 10593−10616.

(14) Krishna, R.; van Baten, J. M. A comparison of the CO_2 capture characteristics of zeolites and metal-organic frameworks. *Sep. Purif. Technol.* **2012**, *87*, 120−126.

(15) Krishna, R. Methodologies for Screening and Selection of Crystalline Microporous Materials in Mixture Separations. *Sep. Purif. Technol.* **2018**, *194*, 281−300.
(16) Hudson, M. R.; Murray, L.; Mason, J. A.; Fickel, D. W.; Lobo, R. F.; Queen, W. L.; Brown, C. M. Unconventional and Highly Selective CO_2 Adsorption in Zeolite SSZ-13. *J. Am. Chem. Soc.* **2012**, *134*, 1970−1973.
(17) Gholipour, F.; Mofarahi, M. Adsorption Equilibrium of Methane and Carbon Dioxide on Zeolite13X: Experimental and Thermodynamic Modeling. *J. Supercrit. Fluids* **2016**, *111*, 47−54.
(18) Hefti, M.; Marx, D.; Joss, L.; Mazzotti, M. Adsorption Equilibrium of Binary Mixtures of Carbon Dioxide and Nitrogen on Zeolites ZSM-5 and 13X. *Microporous Mesoporous Mater.* **2015**, *215*, 215−228.
(19) Mofarahi, M.; Gholipour, F. Gas Adsorption Separation of CO_2/CH_4 System using Zeolite 5A. *Microporous Mesoporous Mater.* **2014**, *200*, 47−54.
(20) Bae, T.-H.; Hudson, M. R.; Mason, J. A.; Queen, W. L.; Dutton, J. J.; Sumida, K.; Micklash, K. J.; Kaye, S. S.; Brown, C. M.; Long, J. R. Evaluation of Cation-exchanged Zeolite Adsorbents for Post-combustion Carbon Dioxide Capture. *Energy Environ. Sci.* **2013**, *6*, 128−138.
(21) Jiang, Y.; Ling, J.; Xiao, P.; He, Y.; Zhao, Q.; Chu, Z.; Liu, Y.; Li, P.; Webley, P. A. Simultaneous Biogas Purification and CO_2 capture by Vacuum Swing Adsorption using Zeolite NaUSY. *Chem. Eng. J.* **2018**, *334*, 2593−2602.
(22) Bower, J.; Barpaga, D.; Prodinger, S.; Krishna, R.; Schaef, H. T.; McGrail, B. P.; Derewinski, M. A.; Motkuri, R. K. Dynamic Adsorption of CO_2/N_2 on Cation-exchanged Chabazite SSZ-13: A Breakthrough Analysis. *ACS Appl. Mater. Interfaces* **2018**, *10*, 14287−14291.
(23) Yang, R. T. *Adsorbents: Fundamentals and Applications*. John Wiley & Sons, Inc.: Hoboken, New Jersey, 2003; pp. 1−410.
(24) Yang, J.; Shang, H.; Krishna, R.; Wang, Y.; Ouyang, K.; Li, J. Adjusting the Proportions of Extra-framework K^+ and Cs^+ cations to Construct a "Molecular Gate" on ZK-5 for CO_2 Removal. *Microporous Mesoporous Mater.* **2018**, *268*, 50−57.
(25) Prats, H.; Bahamon, D.; Giménez, X.; Gamallo, P.; Sayós, R. Computational simulation study of the influence of faujasite Si/Al ratio on CO_2 capture by temperature swing adsorption. *J. CO2 Util.* **2017**, *21*, 261−269.
(26) Prats, H.; Bahamon, D.; Alonso, G.; Giménez, X.; Gamallo, P.; Sayós, R. Optimal Faujasite structures for post combustion CO_2 capture and separation in different swing adsorption processes. *J. CO2 Util.* **2017**, *19*, 100−111.
(27) Koh, D.-Y.; Pimentel, B. R.; Babu, V. P.; Stephenson, N.; Chai, S. W.; Rosinski, A.; Lively, R. P. Sub-ambient air separation via Li^+ exchanged zeolite. *Microporous Mesoporous Mater.* **2018**, *256*, 140−146.
(28) Fu, Y.; Liu, Y.; Li, Z.; Zhang, Q.; Yang, X.; Zhao, C.; Zhang, C.; Wang, H.; Yang, R. T. Insights into adsorption separation of N_2/O_2 mixture on FAU zeolites under plateau special conditions: A molecular simulation study. *Sep. Purif. Technol.* **2020**, *251*, 117405.
(29) Arora, A.; Faruque Hasan, M. M. Flexible oxygen concentrators for medical applications. *Sci. Rep.* **2021**, *11*, 14317.
(30) Vemula, R. R.; Urich, M. D.; Kothare, M. V. Experimental design of a "Snap-on" and standalone single-bed oxygen concentrator for medical applications. *Adsorption* **2021**, *27*, 619−628.
(31) Ruthven, D. M.; Farooq, S.; Knaebel, K. S. *Pressure swing adsorption*. VCH Publishers: New York, 1994; pp. 1−352.
(32) Krishna, R. A Maxwell-Stefan-Glueckauf Description of Transient Mixture Uptake in Microporous Adsorbents. *Sep. Purif. Technol.* **2018**, *191*, 392−399.
(33) Krishna, R. Highlighting the Influence of Thermodynamic Coupling on Kinetic Separations with Microporous Crystalline Materials. *ACS Omega* **2019**, *4*, 3409−3419.
(34) Krishna, R. Maxwell-Stefan Modelling of Mixture Desorption Kinetics in Microporous Crystalline Materials. *Sep. Purif. Technol.* **2019**, *229*, 115790.
(35) Krishna, R. Metrics for Evaluation and Screening of Metal-Organic Frameworks for Applications in Mixture Separations. *ACS Omega* **2020**, *5*, 16987−17004.
(36) van Zandvoort, I.; Ras, E.-J.; de Graaf, R.; Krishna, R. Using Transient Breakthrough Experiments for Screening of Adsorbents for Separation of C_2H_4/CO_2 Mixtures. *Sep. Purif. Technol.* **2020**, *241*, 116706.
(37) Rangnekar, N.; Mittal, N.; Elyassi, B.; Caro, J.; Tsapatsis, M. Zeolite Membranes −A Review and Comparison with MOFs. *Chem. Soc. Rev.* **2015**, *44*, 7128−7154.
(38) Baker, R. W. *Membrane Technology and Applications*. 3rd Edition, John Wiley: New York, 2012.
(39) Krishna, R.; van Baten, J. M. Investigating the potential of MgMOF-74 membranes for CO_2 capture. *J. Membr. Sci.* **2011**, *377*, 249−260.
(40) Krishna, R.; van Baten, J. M. Maxwell-Stefan modeling of slowing-down effects in mixed gas permeation across porous membranes. *J. Membr. Sci.* **2011**, *383*, 289−300.
(41) Krishna, R.; van Baten, J. M. Using the Spreading Pressure to Inter-Relate the Characteristics of Unary, Binary and Ternary Mixture Permeation across Microporous Membranes. *J. Membr. Sci.* **2022**, *643*, 120049.
(42) Krishna, R. Using the Maxwell-Stefan formulation for Highlighting the Influence of Interspecies (1-2) Friction on Binary Mixture Permeation across Microporous and Polymeric Membranes. *J. Membr. Sci.* **2017**, *540*, 261−276.
(43) Algieri, C.; Drioli, E. Zeolite membranes: Synthesis and applications. *Sep. Purif. Technol.* **2021**, *278*, 119295.
(44) Ruthven, D. M. *Principles of Adsorption and Adsorption Processes*. John Wiley: New York, 1984; pp. 1−433.
(45) Myers, A. L.; Prausnitz, J. M. Thermodynamics of Mixed Gas Adsorption. *AIChE J.* **1965**, *11*, 121−130.
(46) Talu, O.; Myers, A. L. Rigorous Thermodynamic Treatment of Gas-Adsorption. *AIChE J.* **1988**, *34*, 1887−1893.
(47) Siperstein, F. R.; Myers, A. L. Mixed-Gas Adsorption. *AIChE J.* **2001**, *47*, 1141−1159.
(48) Krishna, R. Thermodynamic Insights into the Characteristics of Unary and Mixture Permeances in Microporous Membranes. *ACS Omega* **2019**, *4*, 9512−9521.
(49) Krishna, R.; Van Baten, J. M. Using Molecular Simulations to Unravel the Benefits of Characterizing Mixture Permeation in Microporous Membranes in Terms of the Spreading Pressure. *ACS Omega* **2020**, *5*, 32769−32780.
(50) Krishna, R. Thermodynamically Consistent Methodology for Estimation of Diffusivities of Mixtures of Guest Molecules in Microporous Materials. *ACS Omega* **2019**, *4*, 13520−13529.
(51) Krishna, R.; van Baten, J. M. Investigating the Relative Influences of Molecular Dimensions and Binding Energies on Diffusivities of Guest Species Inside Nanoporous Crystalline Materials. *J. Phys. Chem. C* **2012**, *116*, 23556−23568.
(52) Krishna, R.; van Baten, J. M. Influence of Adsorption Thermodynamics on Guest Diffusivities in Nanoporous Crystalline Materials. *Phys. Chem. Chem. Phys.* **2013**, *15*, 7994−8016.
(53) Robeson, L. M. The upper bound revisited. *J. Membr. Sci.* **2008**, *320*, 390−400.
(54) Himma, N. F.; Wardani, A. K.; Prasetya, N.; Aryanti, P. T. P.; Wenten, I. G. Recent progress and challenges in membrane based O_2/N_2 separation. *Rev. Chem. Eng.* **2019**, *35*, 591−625.

https://doi.org/10.1021/acsomega.2c00427
ACS Omega 2022, 7, 13050−13056